Passive Wireless Vibration Sensors Based on the Amplitude Modulation of Harmonic Backscattering

Valentina Palazzi, *Senior Member, IEEE*, Federico Alimenti, *Senior Member, IEEE*, Paolo Mezzanotte, *Member, IEEE*, Manos M. Tentzeris, *Fellow, IEEE*, and Luca Roselli, *Fellow, IEEE*

***Abstract*— This article presents a wireless passive vibration sensor based on harmonic backscattering. The adopted vibration transducer is a commercial piezoelectric cantilever. The cantilever is connected to the gate of an NMOS transistor, which controls the self-bias point of the Schottky diode responsible for the second-harmonic generation. This way, vibrations induce the amplitude modulation of the backscattered second harmonic. A technique is presented to retrieve the vibration information (both acceleration and frequency) from the acquired spectrum. The vibration frequency is computed as the average frequency difference between the carrier and the first sidebands, while the vibration acceleration is encoded in the duty cycle of the amplitude modulation of the backscattered harmonic. In this contribution, we demonstrate for the first time that this information can be retrieved from the magnitude ratio of the first and second sidebands of the acquired spectrum regardless of the tag-to-reader distance. A complete wireless prototype, working at $f_0 = 1.5$ GHz, is manufactured and tested in a laboratory environment for tag-to-reader distances up to 1.3 m. Despite some sensor limitations, i.e., the nonlinear relationship between the duty cycle and the vibration acceleration and the dependence of the sensor sensitivity on the vibration frequency, excellent results are obtained for vibration frequencies around the natural oscillation frequency of the cantilever (i.e., 130 Hz), and for variable accelerations and distances, which testifies the high sensitivity and the robustness of the proposed solution.**

***Index Terms*— Backscatter radio, harmonic backscattering, harmonic transponder, Internet of Things, piezoelectric cantilever, vibration measurement, vibration sensor, wireless sensor.**

I. Introduction

INTERNET of Things (IoT) solutions are more and more used in industrial applications to perform condition monitoring and predictive maintenance of industrial equipment, with the aim to optimize resource usage, reduce waste, and improve safety [1]. Wireless sensors, in particular, are the backbone of IoT systems, as they conveniently provide the required real-time data to decision-making algorithms and to dynamic digital models [2], [3].

Among wireless sensors for industrial applications, vibration sensors play a pivotal role. They are used to perform structural health monitoring (SHM), which is critical to predict risks by checking the wear status of equipment and infrastructures and the stress that mechanical parts are subject to [4]. Vibration sensors are based on a variety of transducers, ranging from piezoelectric and piezoresistive materials [5], [6], to micro-electro mechanical (MEMS) accelerometers [7], [8], strain gauges [9], fiber optics [10], and variable capacitors [11].

The sensor node usually includes the vibration transducer and an active signal conditioning circuit, meaning that an external energy source (usually a battery) is required to power the active circuitry [4]. In addition, energy is needed for wireless communication. However, battery-operated wireless vibration sensors are inconvenient. The weight of the battery can alter the dynamic behavior of the structure to be monitored. In addition, batteries must be replaced periodically, which is an issue for sensors not directly accessible. This is usually the case of vibration sensors, as they can be installed on large tall structures, and inside industrial equipment. In the latter case, periodical battery replacements may cause direct interaction with the monitored equipment and additional costs due to the involvement of dedicated personnel.

For these reasons, research is focusing on developing low-power or even passive wireless vibration sensors [12]. In this context, wireless transponders based on backscatter radios are currently being developed [13], [14], [15]. Backscatter radios are interrogated by wireless signals generated by a reader and they modulate the reflected signals based on the information to be conveyed. This way, they can communicate wirelessly without generating any radio signal on board, which drastically reduces the power consumption for the wireless node [16]. Several attempts are reported in the literature to make backscatter radios energy autonomous, and to extend their read range [17], [18], while making them monitor physical parameters of interest [19]. Additional problems of backscatter radios are self-jamming and self-interference [20], [21], [22], and a few studies are reported, aimed at shifting

Manuscript received 23 June 2023; revised 15 September 2023 and 25 October 2023; accepted 31 October 2023. This work was supported in part by the ECSEL Joint Undertaking (JU) under Grant 876362, in part by the European Union's Horizon 2020 Research and Innovation Program, and in part by Finland, Austria, Belgium, Czechia, Germany, Italy, Latvia, Netherlands, Poland, Switzerland. *(Corresponding author: Valentina Palazzi.)*

Valentina Palazzi, Federico Alimenti, Paolo Mezzanotte, and Luca Roselli are with the Department of Engineering, University of Perugia, 06125 Perugia, Italy (e-mail: valentina.palazzi@unipg.it).

Manos M. Tentzeris is with the School of Electrical and Computer Engineering, Georgia Institute of Technology, Atlanta, GA 30339 USA.

Color versions of one or more figures in this article are available at https://doi.org/10.1109/TMTT.2023.3330759.

Digital Object Identifier 10.1109/TMTT.2023.3330759

the spectrum of the backscattered signal to different frequency bands with respect to the transmitted carrier [23], [24].

A few vibration sensing solutions have been explored based on various types of backscatter radios [25], [26], [27], [28], [29]. In [25], a wireless vibration sensor is proposed based on a strain gauge and a voltage-controlled oscillator (VCO). The strain gauge determines the output voltage of an operational amplifier used to control the oscillation frequency of the VCO (the oscillation frequency is proportional to the strain signal), which, in turn, controls the impedance switching circuit used to modulate the backscattered signal. Therefore, the vibration frequency is encoded as the frequency of the amplitude-modulated backscattered signal. Analogously, the wireless sensor in [26] is based on a microstrip patch antenna and an amplitude modulator powered by a light-power energy harvester, where the resonant frequency of the antenna is a function of the tensile strain applied. However, both the circuit solutions need an additional energy source to operate, which is provided by a solar energy harvester, and therefore, they might not be suitable for environments with dim light conditions, although solar cells optimized for indoor applications are currently being studied [30].

In [27], a surface acoustic wave (SAW) passive wireless vibration sensor is proposed, based on an Y-cut quartz cantilever beam with a proof mass at the free end. Vibrations flex the cantilever, inducing relative changes in the acoustic propagation through the SAW resonators deposited on the surface of the beam and causing a frequency variation in the generated output electromagnetic signal. However, SAW tags are usually more expensive than transponders based on the traditional printed circuit boards (PCBs) and commercial off-the-shelf components and can have limited read range [31].

The wireless passive vibration sensor illustrated in [28], instead, is an LC resonant circuit based on a constant square inductor and a variable parallel-plate capacitor with a movable plate. The LC circuit is magnetically coupled to the reader coil. Under vibration, the capacitance changes due to the motion of the movable plate, which changes the reflection coefficient at the input of the reader coil. In this solution, though, the allowed tag-to-reader distance is extremely limited (in the order of 2 mm).

Among backscatter radios, harmonic transponders are attracting growing interest. Harmonic transponders convert the interrogating signal into its second harmonic, which is then backscattered. Since the backscattered signal lies in a different band with respect to the interrogating signal, the sensitivity of the receiver is not affected by eventual leakage of f_0 signal from the transmitter, or by signal reflections from the environment, like in traditional backscatter radios. Therefore, high receiver sensitivities can be achieved [32]. The sensitivity of harmonic receivers can be impaired by the spurious second harmonic of the transmitter; however, this contribution can be minimized by adding a low-pass filter between the signal generator and the transmitting antenna. Harmonic transponders able to work with radio frequency (RF) input powers as low as -30 dBm have been designed and demonstrated [33]. The higher sensitivity of the receiver and of the tag compensate for the power loss caused by the frequency conversion (variable contribution, depending on the RF input power, the diode nonlinearity, and the circuit status [34]) and the higher path loss experienced by the backscattered second harmonic with respect to the fundamental tone (6-dB additional loss), leading to wireless sensing systems with potential longer read ranges than the traditional backscatter radios, especially in highly cluttered environments. In addition, their inherent immunity to clutter makes harmonic transponders good candidates for high-sensitivity sensors, and currently research has focused on adding sensing capabilities to harmonic transponders [35], [36], [37], [38], [39].

In [29], two circuit implementations for vibration sensing are presented based on harmonic backscattering. In the first circuit, a piezoelectric cantilever is used to change the bias point of a GaAs diode, leading to an amplitude modulation of the output signal. However, the impedance seen by the cantilever is lower than the optimal one, which leads to poor sensitivity. In the second circuit type, a mechanical switch is used to open and close the diode dc current path at the doubler input. Such a circuit can be used to detect low-frequency vibrations; however, the vibration acceleration cannot be measured.

In the present study, a wireless passive vibration sensor based on harmonic backscattering is presented, where a piezoelectric cantilever is used to switch an NMOS transistor between OFF and triode region. Both vibration acceleration and frequency can be recovered from the backscattered signal regardless of the tag-to-reader distance, using a mix of the two approaches described in [29]. This article is organized as follows. The theory of operation is shown in Section (II). Section III is dedicated to discuss the experimental results, and finally the conclusions are drawn.

II. Theory of Operation

This article describes a wireless passive vibration sensor suitable for condition monitoring. The transponder relies on harmonic backscattering: a reader interrogates the tag using a sinusoidal signal with frequency f_0, while the tag backscatters the signal at the second harmonic [33]. The sensor induces the amplitude modulation of the harmonic backscattered signal, without requiring any additional energy source. Thanks to the frequency separation between the transmitted and received signals, harmonic transponders are robust to clutter, which makes them preferable in industrial environments [40].

The key component of the proposed transponder is a passive frequency doubler, which is shown in Fig. 1. The frequency doubler is a two-port network which aims at converting the RF input signal at the fundamental frequency f_0 into its second harmonic at $2f_0$. It is composed of a series-connected low-barrier Schottky diode (nonlinearity), two quarter-wave stubs at f_0 (harmonic filters) connected in shunt at the two sides of the diode, and the input and output matching networks (the circuit is designed for source and load impedances of 50 Ω).

In the state-of-the-art frequency doubler in [41], the output matching network is composed of an LC network, where the inductor (see L_m in Fig. 1) and the capacitor (see C_m in Fig. 1) also provide a return path for the self-generated dc component. Indeed, when a sinusoidal signal is applied to a Schottky diode,

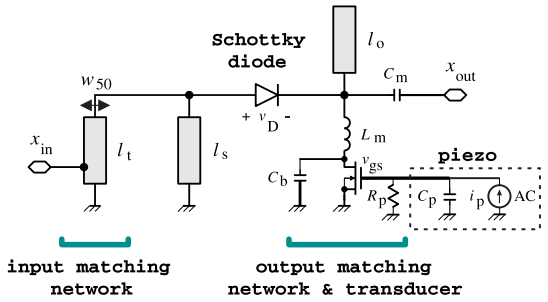

Fig. 1. Schematic of the proposed frequency doubler. The main parameters are: $w_{50} = 1.62$ mm, $l_t = 25.8$ mm, $l_s = 29.7$ mm, $l_s = l_o = 29.7$ mm, $C_m = 0.4$ pF, $L_m = 4.6$ nH, $C_b = 50$ pF, and $C_p = 22$ nF.

a dc component is generated along with the higher harmonic components [33], [34]. The series capacitor C_m prevents the dc component from entering the output load. On the other hand, the short-circuited harmonic stub, connected to the diode anode, and the inductor L_m, connected to ground, form a closed path where the self-generated dc current can circulate, while the dc voltage across the diode is forced to zero, i.e., the diode is zero-biased.

In the present modified version of the frequency doubler, a low-frequency NMOS transistor switch is connected between the inductance L_m and ground. The gate of the transistor is used to modulate the amplitude of the generated second-harmonic signal (hence called "modulation port"), by controlling the only dc component generated by the diode [34]. A bypass capacitor C_b is connected in parallel between the drain terminal of the transistor and ground, so that the transistor state only affects the self-generated dc component (L_m is RF-connected to ground). This way, the switch parasitics do not affect the behavior of the frequency doubler.

When the gate–source voltage V_{gs} is above the threshold voltage of the transistor V_{th}, the transistor is in the triode region and the channel is formed. Therefore, the inductance is dc-connected to ground and the Schottky diode is zero-biased (ON state); in this case, the maximum RF power is generated and transmitted to the output port of the frequency doubler.

When the gate–source voltage is below threshold, the channel is not formed instead, L_m is not dc-connected to ground, and the dc current is zero. In this case, it can be demonstrated that a positive voltage is developed at the diode cathode, and that the diode is reverse-biased. In particular, the dc voltage across the diode $v_{D,dc}$ can be expressed as a function of the diode voltage at the fundamental frequency $v_{D,f0}$ as follows [34]:

$$v_{D,\mathrm{dc}} = -nV_T \ln\left[I_0\left(\frac{v_{D,f0}}{nV_T}\right)\right] \tag{1}$$

where I_0 is the modified Bessel function of the first kind of the zeroth order, n is the diode ideality factor, and V_T is the thermal voltage. Since $I_0(x)$ is a positive monotonically increasing function of $x = v_{D,f0}/(nV_T)$, $v_{D,dc}$ is negative, meaning that the diode is reverse-biased. In this condition, the power of the generated second harmonic is significantly reduced (OFF state). It is worth noting that in the proposed circuit the diode is never forward-biased, since no external bias is applied to the diode. Therefore, the frequency doubler has the minimum conversion loss when the diode is zero-biased.

A piezoelectric cantilever is connected to the NMOS transistor to implement a passive wireless vibration sensor, as shown in Fig. 1. The piezoelectric cantilever can be modeled as a current source i_p in parallel with a capacitor C_p [5], [42]. Under vibration, the piezoelectric cantilever develops a time-varying voltage v_{gs} between the gate and the source of the MOSFET. For simplicity, sinusoidal vibrations are considered in this analysis, which leads to a sinusoidal voltage signal generated by the piezoelectric cantilever. The frequency of the generated signal depends on the vibration frequency f_v, and, for a given vibration frequency, its amplitude V_{gs} depends on the vibration acceleration a_v (the higher the vibration acceleration, the higher the voltage generated by the piezoelectric cantilever). Therefore, the voltage signal at the gate of the transistor can be expressed as follows:

$$v_{gs}(t) = V_{gs}\cos(2\pi f_v t + \phi_0) \tag{2}$$

where ϕ_0 is the initial phase of the signal. Thanks to the high impedance at the gate port of the transistor ($C_{gs} \approx 50$ pF), a very small power is needed to switch ON and OFF the NMOS transistor switch [34], which can be easily provided by the piezoelectric cantilever [43]. A 1 MΩ resistor (R_p in Fig. 1) is connected in parallel with the cantilever to have a path to periodically discharge the capacitor C_{gs} based on the voltage applied by the cantilever.

When the voltage signal applied to the gate of the transistor is above a given threshold voltage, the switch is closed and the frequency doubler is in the ON state, while when the voltage is below threshold (including negative voltages) the transistor switch is open and the frequency doubler is in the OFF state. The fraction of the vibration period in which the frequency doubler is ON or OFF depends on the threshold voltage V_{th} and ON the amplitude of the voltage signal V_{gs}, as shown by Fig. 2(a). Let us define the duty cycle D of the amplitude-modulated second harmonic as follows:

$$D = \frac{T_{\mathrm{ON}}}{T_v} \tag{3}$$

where T_{ON} is the time interval in which the transistor switch is ON, and $T_v = 1/f_v$ is the vibration period.

Sinusoidal signals with larger amplitudes, corresponding to larger accelerations, lead to larger duty cycles. Indeed, D, V_{gs}, and V_{th} are related as follows:

$$D = \frac{1}{\pi}\arccos\left(\frac{V_{\mathrm{th}}}{V_{\mathrm{gs}}}\right). \tag{4}$$

On a first approximation, the output signal x_{out} can be modeled as the second harmonic generated by the diode multiplied by a square wave with period T_v and duty cycle D

$$x_{\mathrm{out}} = \cos(2\omega_0 t)\left[A_{\mathrm{avg}} + (A_{\mathrm{ON}} - A_{\mathrm{OFF}})\sum_{n=1}^{\infty} a_n \cos(n\omega_v t)\right] \tag{5}$$

where

$$A_{\mathrm{avg}} = A_{\mathrm{ON}}D + A_{\mathrm{OFF}}(1 - D). \tag{6}$$

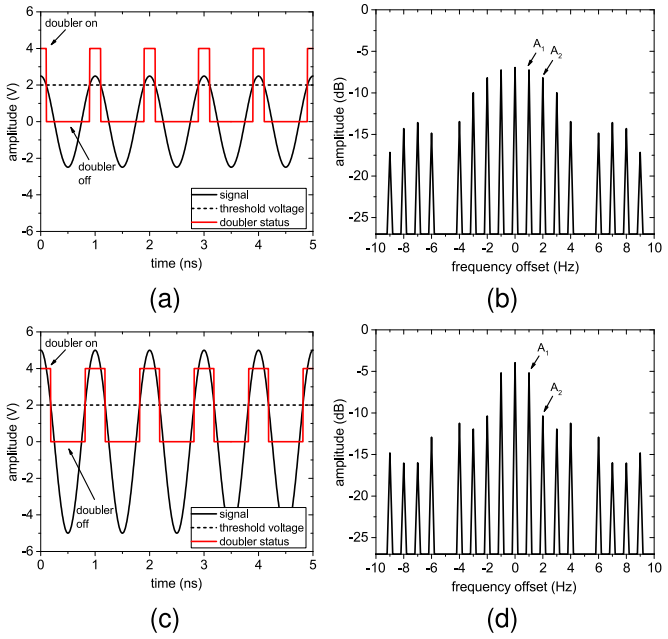

Fig. 2. Dependence of the duty cycle of the amplitude-modulated second harmonic on the amplitude of the signal generated by the piezoelectric transducer: (a) and (b) 20% duty cycle and (c) and (d) 40% duty cycle. (a) and (c) Time-domain signals generated by the piezoelectric cantilever and (b) and (d) output spectra. For simplicity, (b) and (d) are generated assuming $A_{\mathrm{ON}} = 1$ V, $A_{\mathrm{OFF}} = 0$ V, and the x-axis is normalized with respect to the carrier frequency.

A_{ON} is the amplitude of the RF output signal when the switch is closed (the so-called "ON" state), A_{OFF} is the amplitude of the RF output signal when the switch is open (the so-called "OFF" state), $\omega_0 = 2\pi f_0$, $\omega_v = 2\pi f_v$, and

$$a_n = \frac{2}{n\pi} \sin(n\pi D) \tag{7}$$

are the Fourier coefficients of the square wave.

The Fourier transform of x_{out} corresponds to the convolution of the Fourier transform of the sinusoidal RF signal and the square wave, as follows:

$$X_{\mathrm{out}}(f) = A_0\delta(f - 2f_0) + \sum_{n=1}^{\infty} A_n\delta(f - 2f_0 \pm nf_v) \tag{8}$$

where

$$A_0 = \frac{A_{\mathrm{avg}}}{2} \tag{9}$$

and

$$A_n = \frac{(A_{\mathrm{ON}} - A_{\mathrm{OFF}})a_n}{4}. \tag{10}$$

Generally, we need both magnitude and phase of the Fourier transform of x_{out} to retrieve the time-domain signal, since the spectral lines associated with the generated sidebands are multiplied by coefficients a_n that can be positive or negative based on the sign of the term $\sin(n\pi D)$.

In the present contribution, a method is proposed to retrieve the RF output signal x_{out} from the only spectrum acquired by the receiver. This method leverages the fact that the duty cycle of the square wave is always below 50% (the sinusoidal voltage generated by the piezoelectric cantilever is negative for half of its period, which implies it is below the threshold voltage of the transistor). Therefore, the coefficients associated with the first and second sidebands (A_1 and A_2) are necessarily positive, and their ratio A_{21} is equal to

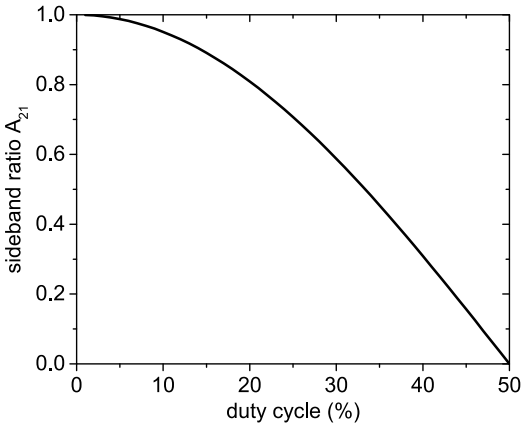

Fig. 3. Ratio of the magnitude of the second sideband (component at $f_0 \pm 2f_v$) to the first sideband (component at $f_0 \pm f_v$) A_{21} versus the duty cycle of the square wave D for practical $0 < D < 0.5$.

$$A_{21} = \frac{A_2}{A_1} = \frac{a_2}{a_1} = \frac{1}{2}\frac{\sin(2\pi D)}{\sin(\pi D)}. \tag{11}$$

For $D < 0.5$, $D \neq 0$, this is a positive, monotonically decreasing function of D, as shown in Fig. 3. Therefore, we can associate a unique D value with each A_{21} value, and A_{21} can be used to measure the vibration acceleration. Fig. 2(b) and (d) shows the spectrum associated with a duty cycle of 20% and 40%, respectively, clearly indicating the components A_1 and A_2. It can be noted that A_{21} does not depend on A_{ON} and A_{OFF}; therefore, this parameter is independent of the RF input power, which makes the proposed transducer and acquisition method generically suitable for wireless transponders.

Once D is known, the sign of all the sidebands can be calculated using (7), and the time-domain signal can be reconstructed. A preliminary characterization of the system is needed to associate the measured duty cycle values to vibration accelerations for each vibration frequency. This way, the vibration acceleration can be directly related to D.

It is worth mentioning that some approximations were made: when V_{gs} is equal to the transistor threshold voltage, the resistance between the drain and source is still high. The voltage drop across it is significant, and the diode is still reverse-biased, which implies that the frequency doubler is not in the ON state yet. As V_{gs} increases, this resistance decreases, and also the voltage potential developed across the resistance decreases. Therefore, a transition region is expected, where P_{out} features intermediate values between the ON and the OFF states. The threshold voltage V_{th} that separates the ON from the OFF state of the frequency doubler is defined as the gate–source voltage which minimizes the error caused by the approximation of the measured output power $P_{\mathrm{out,meas}}$ with the theoretical step function $P_{\mathrm{out,th}}$. Assuming P_{out} is evaluated for a number N of gate–source voltage samples from the OFF to the ON state at steps ΔV_{gs}, the threshold voltage

V_{th} is defined as follows:

$$V_{\text{th}} = \arg\min_{V_{\text{gs}}} \text{err}_{P\text{out}} \tag{12}$$

where

$$\text{err}_{P\text{out}} = \frac{\sum_{n=1}^{N} \left| P_{\text{out,dB,meas}}(n) - P_{\text{out,dB,th}}(n) \right| \dot{\Delta} V_{\text{gs}}}{N}. \tag{13}$$

As a result, the threshold voltage defined to separate the ON and OFF states of the frequency doubler does not correspond exactly to the threshold voltage of the transistor, and it is actually slightly higher than that.

A significant advantage of the proposed approach is that the whole information on the vibration (i.e., both frequency and acceleration) can be retrieved from the analysis of just the carrier and the first two sidebands of the spectrum of the output signal. However, it is worth mentioning that since the vibration simply causes the amplitude modulation of the backscattered second harmonic, the sensor information can be retrieved also using conventional AM receivers tuned to $2f_0$. The proposed method is specifically developed to retrieve frequency and acceleration of sinusoidal vibrations. The estimate of acceleration can be inaccurate if v_{gs} is distorted.

III. Experimental Results

A proof-of-concept prototype of the frequency doubler in microstrip technology was designed and manufactured. The adopted substrate was the Rogers RO4350B ($\epsilon_r = 3.66$, $\tan\delta = 0.0031$, substrate thickness $= 762\ \mu$m). The following off-the-shelf components were used: HSMS2850 from Broadcom was used as the Schottky diode, BSS123 was used as the NMOS transistor, and S129-H5FR-1803YB piezoelectric bending transducer from MIDE was used as the piezoelectric cantilever ($C_p = 22$ nF). The doubler was designed with the CAD Advanced Design System using Harmonic Balance simulations for a fundamental frequency $f_0 = 1.5$ GHz and is optimized to achieve the minimum conversion loss when the inductor L_m is connected to ground for an available input power in the range $[-10, -20]$ dBm. The SPICE model used for the Schottky diode is provided by the manufacturer and includes package parasitics. No reliable SPICE models of the BSS123 were found, so we used an experimental approach. A photograph of the prototype is shown in Fig. 4.

First, we measured the variation in the power at the RF output port of the frequency doubler P_{out} with respect to the voltage applied to the gate of the transistor V_{gs}. We connected the input port of the frequency doubler to an RF signal generator, the output port to a spectrum analyzer, while V_{gs} was varied with a power supply.

The results, obtained for two different values of the available input power P_{in}, are shown in Fig. 5. We can identify two different operating regions of the frequency doubler where P_{out} is constant: an OFF region for $V_{\text{gs}} < 1.4$ V and an ON region for $V_{\text{gs}} > 1.8$ V. For $P_{\text{in}} = -10$ dBm, the conversion loss is equal to 15 dB in the ON region and equal to 31 dB in the OFF region, while for $P_{\text{in}} = -20$ dBm, the conversion loss is equal to 18 dB in the ON region and equal to 31 dB in the OFF region. The threshold voltage of the transistor is equal to 1.4 V.

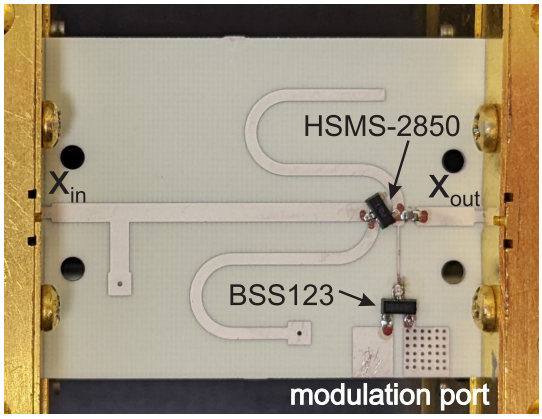

Fig. 4. Photograph of the prototype of the designed frequency doubler for vibration sensing.

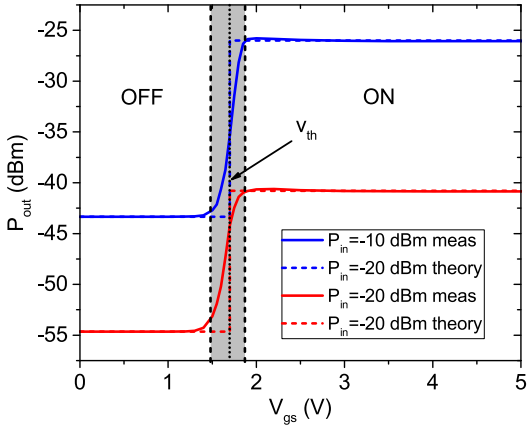

Fig. 5. Measured RF output power versus gate-to-source voltage for different RF input powers.

Between the ON and OFF states, we can see a narrow transition region extending from 1.4 to 1.8 V (in gray in Fig. 5), where the RF output power features intermediate values between the ON and OFF states. As mentioned in Section II, this is due to the fact that at the border of the triode region the resistance measured between the drain and source is still high, and the diode is still reverse-biased. As V_{gs} increases, the drain–source resistance decreases, and also the voltage potential developed across the resistance decreases, thereby increasing P_{out}. Since the graph in Fig. 5 is approximated by an ideal step in the developed theory, we define the threshold voltage that separates the ON from the OFF region of the frequency doubler as the gate–source voltage which minimizes the error caused by the step approximation, as described in (13). Therefore, V_{th} is set to 1.65 V.

We can observe that the RF output power increases by 15 dB from the OFF to the ON state for $P_{\text{in}} = -10$ dBm, and it increases by 12 dB for $P_{\text{in}} = -20$ dBm. The reduced difference between the two states for lower RF input powers is due to the fact that as the RF input power P_{in} decreases, the dc voltage that is self-generated by the diode $v_{D,\text{dc}}$ is smaller, as shown by (1). Therefore, it has a smaller impact on the frequency doubler performance [34]. Nevertheless, this difference is still considerable for RF input powers as low as

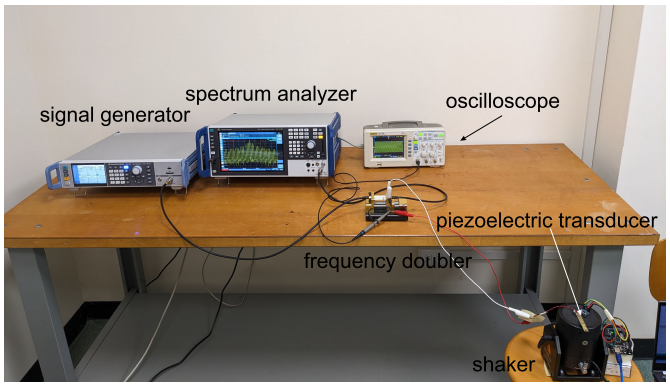

Fig. 6. Proof-of-concept experimental setup for the testing of the frequency-doubler-based sensor using a piezoelectric cantilever.

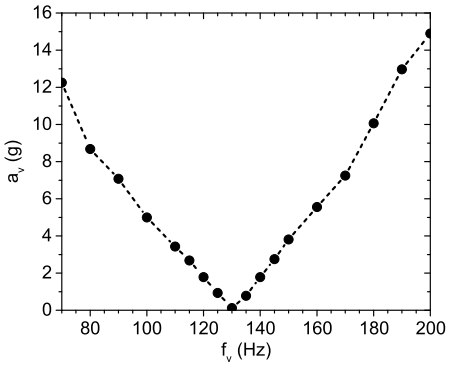

Fig. 7. Cantilever characterization: acceleration corresponding to $V_{gs} = 2$ V for different vibration frequencies.

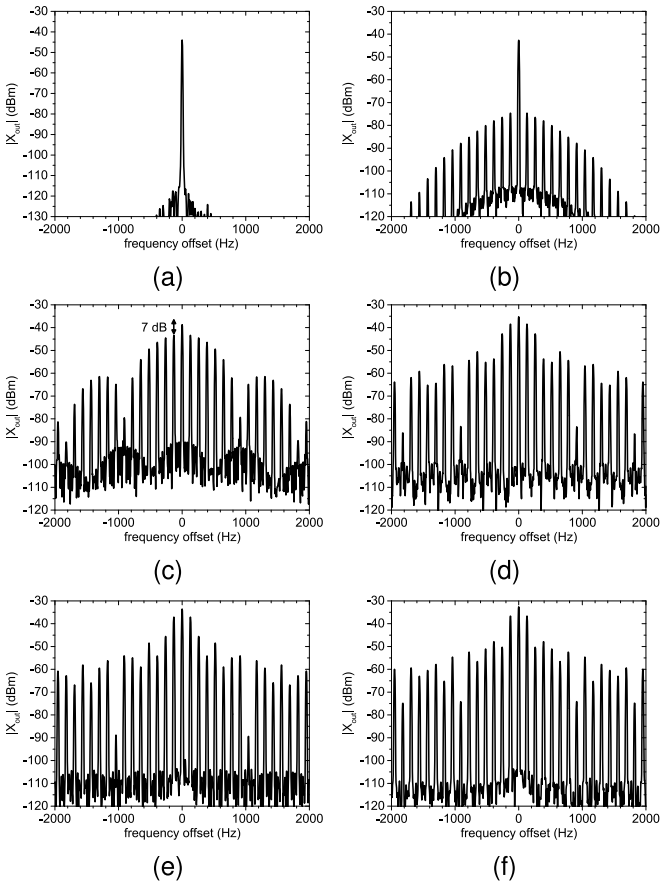

Fig. 8. Measured output spectrum for $f_v = 130$ Hz and $P_{in} = -10$ dBm. (a) $V_{gs} = 0$ V (corresponding to no vibration), (b) $V_{gs} = 1.6$ V, (c) $V_{gs} = 1.9$ V, (d) $V_{gs} = 2.45$ V, (e) $V_{gs} = 4.3$ V, and (f) $V_{gs} = 8$ V.

-20 dBm, which guarantees a high transponder sensitivity for wireless applications. Indeed, assuming $f_0 = 2.45$ GHz (ISM band), in case the power transmitted by the reader is 36 dBm, this sensitivity corresponds to a read range of 9 m.

The setup adopted to test the frequency doubler with a piezoelectric cantilever is shown in Fig. 6. The transistor is connected to the piezoelectric cantilever using two wires. One side of the cantilever is fixed to a shaker (model DS-PM-20 from DEWESoft) with a screw. A commercial accelerometer (model ADXL354 from Analog Devices) is also placed on the shaker next to the cantilever to measure the acceleration of the applied vibration. An oscilloscope voltage probe is connected in parallel with the cantilever to check the voltage waveforms generated by the cantilever in real-time.

First, we characterized the adopted piezoelectric cantilever. The natural oscillation frequency of the cantilever is estimated as the vibration frequency where the lowest acceleration is needed to achieve a certain generated voltage amplitude. The vibration frequency is varied in the range of 70–200 Hz at steps of 5 Hz. The results are shown in Fig. 7 for $V_{gs} = 2$ V (i.e., just above threshold). Based on the results, the estimated natural oscillation frequency is 130 Hz. In this study, we aimed at achieving the highest vibration sensitivity. Therefore, we used the transducer around its resonance.

We analyzed the relationship between the RF signal at the output port of the frequency doubler and the gate-to-source voltage generated by the piezoelectric transducer. The vibration frequency of the shaker is set to 130 Hz. The transmitted RF input power is set to -10 dBm, and the vibration acceleration is varied so that a variable V_{gs} is generated by the piezoelectric cantilever. Sample spectra acquired at the RF output port for different accelerations are shown in Fig. 8. The acquisition band of the spectrum analyzer is set to 4 kHz, the resolution band is 10 Hz, and the number of points is 801. These parameters are set to achieve a satisfactory resolution, low noise floor, while keeping fast sweep time.

A simple MATLAB code is developed to retrieve the vibration information from the spectrum. The code first identifies local maxima in the acquired spectrum using the function `findpeaks`. To avoid false peaks due to noise, all the peaks which are below -100 dBm are disregarded by defining "`MinPeakHeight`," while the minimum distance between two peaks is set to 60 Hz by defining "`MinPeakDistance`." The "`MinPeakHeight`" value is determined heuristically based on the measured noise floor of the spectrum analyzer, while the "`MinPeakDistance`" value is determined based on the operating frequency band of the used piezoelectric transducer. Machine-learning-based estimators can also be used to reduce the risk of errors in noisy signal acquisitions.

If there are no vibrations, no sidebands are present in the spectrum, as shown in Fig. 8(a). If the vibrations are too

weak to generate a voltage above threshold, there might be sidebands in the spectrum, but they are well below the carrier (an example is shown in Fig. 8(b) where $V_{gs} = 1.6$ V and the first sideband is about 20 dB below the carrier). Finally, if the vibrations are strong enough to generate V_{gs} greater than V_{th}, sidebands appear in the spectrum according to the proposed theory. In Fig. 8(c), the first sidebands A_1 are about 7 dB below the carrier and this case can be considered borderline, since V_{gs} is slightly higher than V_{th}. Therefore, for a given vibration frequency, the ratio of the carrier component to the first sideband is computed and the acceleration corresponding to $A_{01} = A_0/A_1 = -7$ dB is set as the lowest acceleration that can be measured by the transponder. As the vibration acceleration increases, the voltage amplitude generated by the piezoelectric cantilever increases as well (the measured values are reported in the caption of Fig. 8), which causes a larger D. Consequently, the amplitude of the carrier increases, since it depends linearly on D, as shown in (9). In addition, the relative amplitude of the sidebands varies.

The vibration frequency is calculated as the average frequency separation between the first sidebands and the carrier tone. Then, the duty cycle D of the waveform is determined from A_{21} as described in (11). To verify the consistency of the process, the signal envelope is also recovered. The Fourier coefficients are calculated as described in (7). Finally, the time-domain waveform is retrieved using (5).

The duty cycle of the modulating signal, retrieved from the acquired spectrum using the parameter A_{21} ("measurements"), is then compared with the duty cycle calculated using (3) ("theory") based on V_{gs} amplitude directly measured with the oscilloscope, as shown in Fig. 9(a). We observe an excellent agreement between the measurements and theory as long as V_{gs} is larger than V_{th}.

The retrieved time-domain modulation signals are shown in Fig. 9(b) and (c) for two different V_{gs}. Square waves with different duty cycles can be clearly identified in both the cases. The retrieved RF signal envelope is confronted with the respective voltage signal v_{gs} generated by the piezoelectric cantilever. We can observe the close correspondence between the fraction of the vibration period in which the voltage signal is above V_{th} and the duty cycle of the signal envelope. The modulation frequency measured with the above-described method is equal to 130 Hz for all the spectra, in perfect agreement with the nominal vibration frequency displayed by the shaker.

The RF output signal is also acquired for different values of the RF input power, for a fixed vibration frequency ($f_v =$ 130 Hz). The results are illustrated in Fig. 10. We can observe a good agreement in the duty cycle estimation in all the cases in Fig. 10(a), while the estimated modulation frequency is the same in all the cases (equal to 130 Hz), as shown by the reconstructed time-domain modulation signals in Fig. 10(b) for $V_{gs} = 7.4$ V.

Then, we analyzed the relationship between the duty cycle of the RF output signal of the frequency doubler and the vibration acceleration. All the piezoelectric transducers are characterized by a frequency response which depends on their shape, weight, and elasticity [44]. Therefore, a calibration step

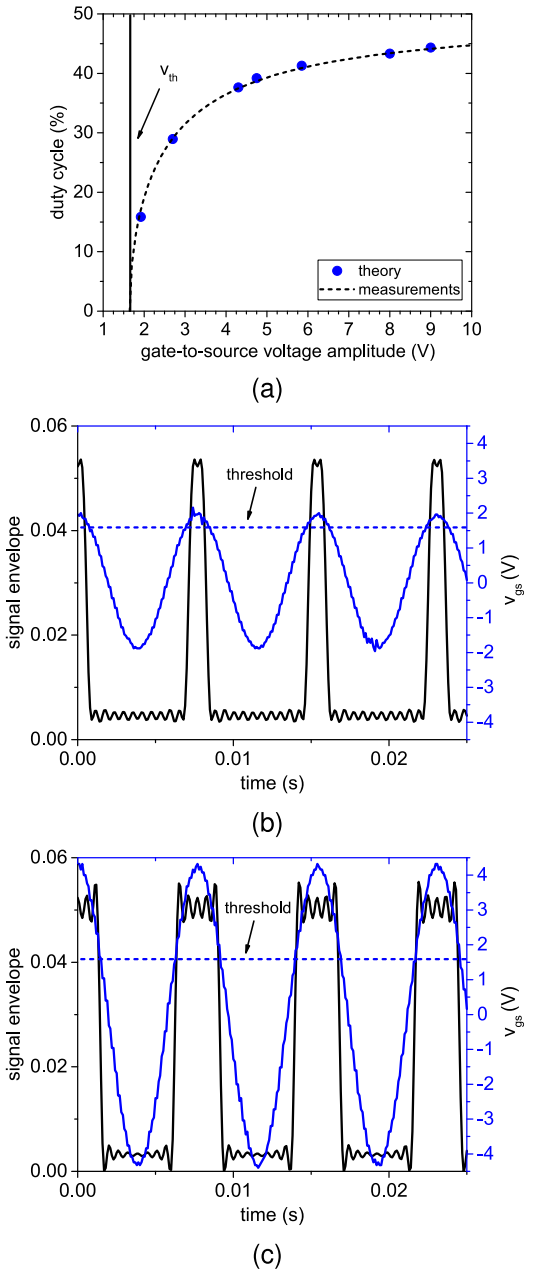

Fig. 9. RF output signals at $f_v = 130$ Hz for different vibration accelerations. (a) Measured duty cycle, (b) retrieved modulation signal and measured gate-to-source voltage for $V_{gs} = 1.9$ V, and (c) for $V_{gs} = 4.3$ V.

is needed to determine the relationship between the measured duty cycle and the vibration acceleration for each vibration frequency. To identify the operating frequency band of the vibration sensor, we set the vibration acceleration to 2 g, and we varied the vibration frequency of the shaker. The measured duty cycles versus vibration frequency are shown in Fig. 11. The tag is able to detect vibrations in the frequency range from 115 to 142 Hz for a vibration acceleration of 2 g. The highest duty cycle is measured at the resonance frequency of the cantilever, namely, at 130 Hz, where the piezoelectric cantilever generates the largest V_{gs}. It is worth mentioning that the operating frequency band of the proposed vibration sensor depends on the adopted piezoelectric cantilever, since

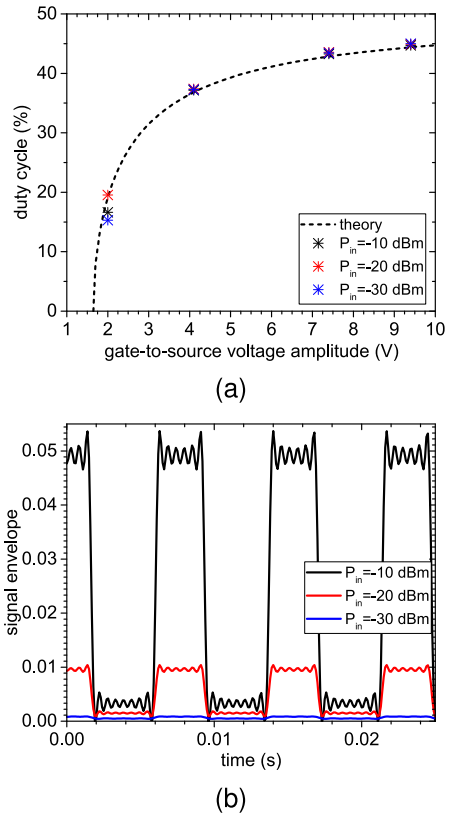

Fig. 10. RF output signals at $f_v = 130$ Hz for different RF input powers. (a) Measured D and (b) retrieved envelopes of the measured modulated signals for $V_{gs} = 7.4$ V.

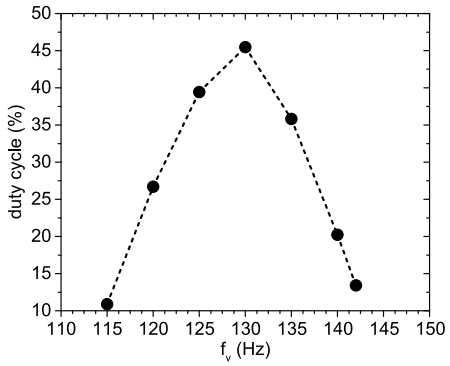

Fig. 11. Measured duty cycle versus vibration frequency (acceleration 2 g).

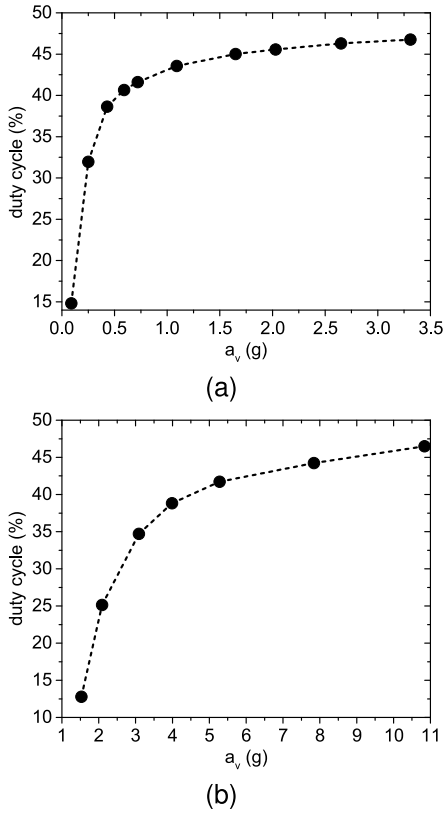

Fig. 12. Measured duty cycle versus vibration acceleration for (a) $f_v = 130$ and (b) $f_v = 120$ Hz.

the proposed circuit can sustain modulation frequencies up to 10 MHz, as already demonstrated in [34]. Therefore, transducers with different natural oscillation frequencies can be used to make the sensor sensitive to different vibration frequencies.

In Fig. 12(a) and (b), the duty cycle of the RF output signal versus the vibration acceleration are shown for two vibration frequencies. In the first case, the vibration frequency of the shaker is set to 130 Hz, and the vibration acceleration is varied. As shown in Fig. 12(a), the measured duty cycle parameter varies from about 14.8% to 46.8% for a vibration acceleration ranging from 0.09 to 3.3 g. The estimated vibration frequency with the developed MATLAB code is 130 Hz in all the cases. The same experiment is repeated for $f_v = 120$ Hz, and the results are shown in Fig. 12(b). The measured duty cycle parameter varies from about 12.8% to 46.5% for a vibration acceleration ranging from 1.5 to 10 g. In both the cases, the relationship D–a_v is nonlinear, and D increases monotonically as a_v increases. The largest vibration frequency that can be sensed by the transducer is limited by the saturation of $D(a_v)$ function. The nonlinear D–a_v relationship makes this transponder a good candidate for shock sensing. Acceleration sensitivity increases significantly close to the natural oscillation frequency of the piezoelecric cantilever, since, for a given acceleration, the cantilever deflection is larger than at any other oscillation frequency, which means that a larger voltage signal is generated. The sensitivity progressively degrades moving away from the resonance, although the acceleration sensing range significantly increases. The transducer should be used at resonance to detect weak vibrations and off resonance to monitor larger accelerations.

These results demonstrate the high sensitivity of the proposed solution and its suitability to perform condition monitoring for electrical machines and industrial equipment [12]. The threshold voltage of the MOSFET impacts on the sensitivity of the sensor, since, for a given piezoelectric transducer, a lower threshold voltage allows the sensor to measure weaker vibrations. If the threshold voltage of the FET is unknown, a calibration step is needed to accurately measure vibration accelerations.

Finally, a complete wireless fully passive sensor—with wireless interrogation capability—was manufactured and tested. The described modulation-capable frequency doubler

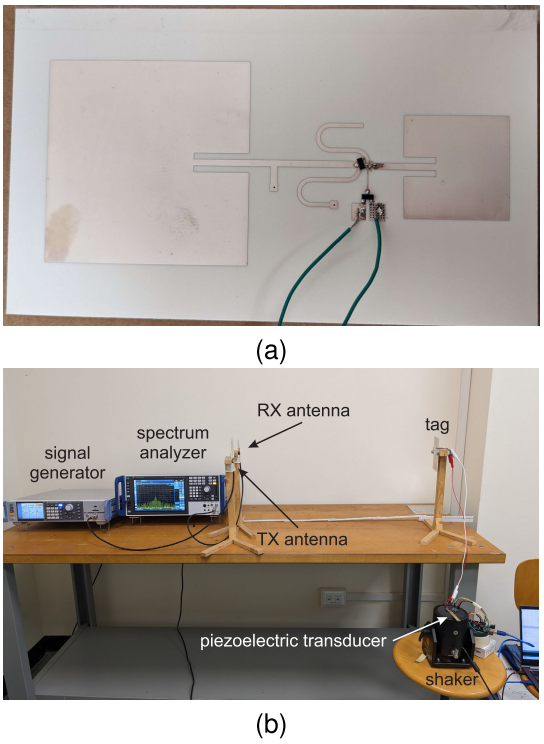

Fig. 13. Test of the wireless vibration sensor: (a) photograph of the tag and (b) experimental setup.

is connected to an antenna working at $f_0 = 1.5$ GHz at the input port, and to an antenna working at $2f_0$ at the output port. A photograph of the manufactured proof-of-concept prototype is shown in Fig. 13(a). Two square patch antennas are used as the radiating elements. The two antennas are matched to 50 Ω, and the whole prototype is manufactured on Rogers 4350B. The overall area of the PCB is 13.5 × 8 cm^2.

The adopted test setup is shown in Fig. 13(b). The signal generator is connected to a patch antenna with its first resonance at f_0 and the spectrum analyzer is connected to a patch antenna with its first resonance at $2f_0$ (the tag and the reader antennas are the same in the adopted proof-of-concept setup). The power transmitted at f_0 is 15 dBm, and the same settings as in the previous experiment are used for the spectrum analyzer (namely, acquisition band 4 kHz, resolution band 10 Hz). The threshold power to avoid spurious peaks in the MATLAB code is lowered to −120 dBm due to the lower noise floor experienced in the wireless experiment due to the weaker received signal.

The vibration frequency of the shaker is set to 130 Hz, and, for each vibration acceleration, the tag-to-reader distance is varied from 50 to 130 cm. The tag-to-reader distance is chosen to have an RF power P_{in} at the input of the doubler in the design range $[-10, -20]$ dBm. The coverage can be further improved by increasing the transmitted power and using an LNA at the receiver input. The measured spectra are illustrated in Fig. 14 for $a_v = 1$ g. As expected, the received power varies depending on the tag-to-reader distance, on the multipath, and so forth. However, the carrier and the first two sidebands, which are needed to recover the sensor information, are still significantly above the noise floor, and the magnitude ratio of

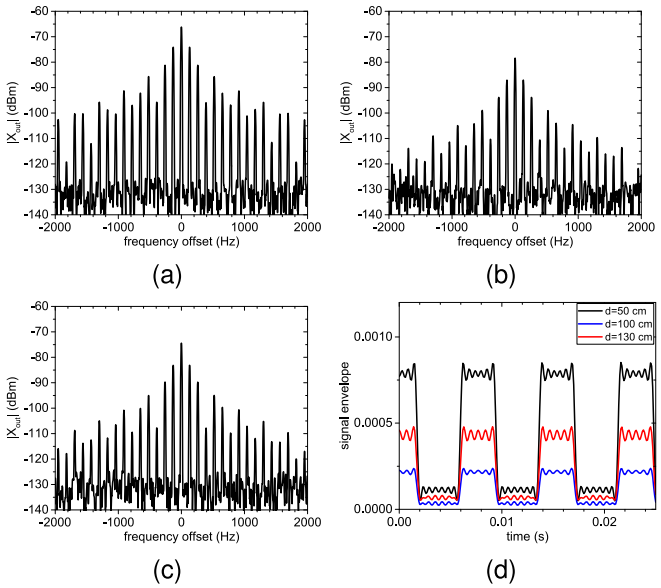

Fig. 14. Received signals versus tag-to-reader distance for $f_v = 130$ Hz and $a_v = 1$ g. (a) Spectrum for $d = 50$ cm, (b) spectrum for $d = 100$ cm, (c) spectrum for $d = 130$ cm, and (d) reconstructed time-domain signal envelope versus distance.

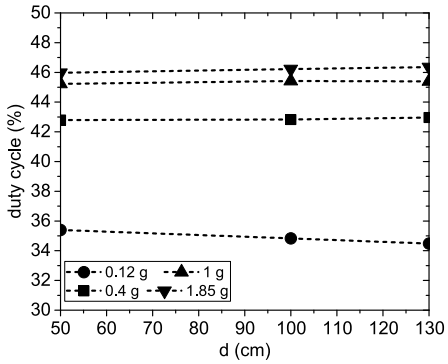

Fig. 15. Measured duty cycle at $f_v = 130$ Hz for different tag-to-reader distances and vibration accelerations.

the first and second sidebands is the same, except for the noise of the acquisition instrument.

The estimated vibration frequency is equal to 130 Hz for all the measurements. Fig. 14(d) shows the reconstructed envelope signals. The square waves are clearly recognizable for all the three distances.

The estimated duty cycle versus distance at $f_v = 130$ Hz is shown in Fig. 15 for different vibration accelerations. We observe that for a given acceleration, the measured duty cycle is almost the same regardless of the tag-to-reader distance. Small fluctuations are due to noise. The noise impact can be mitigated by averaging repeated measurements.

Finally, we tested the capability of the tag to operate in highly cluttered environments and in the presence of dynamic multipath, to test its suitability for industrial environments. Since vibrations induce the amplitude modulation of the backscattered second harmonic, multipath fading can cause the attenuation of single spectral components, thus causing errors in the vibration acceleration estimation. To mitigate this, the estimation of the duty cycle is made by averaging

TABLE I
COMPARISON TO THE STATE OF THE ART

Ref.	passive	transponder type	transducer type	measured parameters	vibr. frequency (Hz)	vibr. acceleration (g)
this work	yes	harmonic tag	piezoelectric cantilever	acceleration and frequency	$115-143$ 120 130	above 2 $1.5-11$ $0.09-3.5$
[25]	no	antenna backscattering	strain gauge	strain	11.9	/
[26]	no	antenna backscattering	microstrip patch	strain	1-8	/
[28]	yes	LC resonator	capacitor	acceleration	120	$0.4-5.1$
[27]	yes	SAW device	piezoelectric cantilever	acceleration and frequency	20	0-2.5
[29]	yes	harmonic tag	piezoelectric cantilever	acceleration and frequency	5-85	9-40
[29]	yes	harmonic tag	mechanical switch	frequency	0.1 30	0.01 2.3

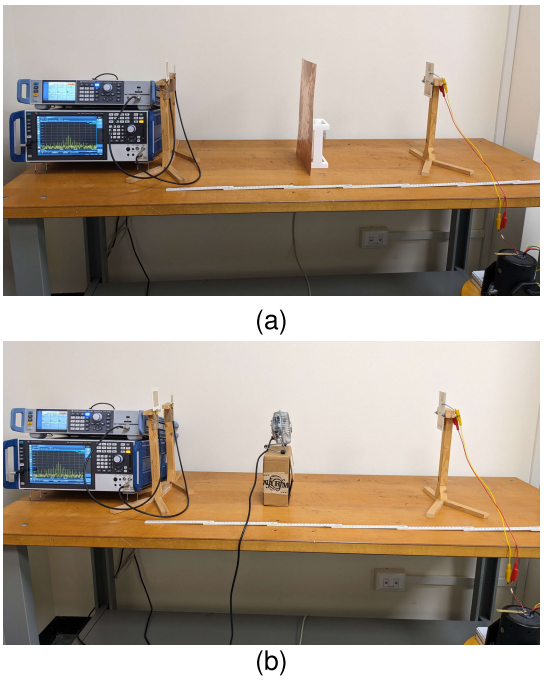

Fig. 16. Experimental setup to test the tag in an environment with clutter and multipath: (a) metal panel between the tag and the reader and (b) rotating fan between the tag and the reader.

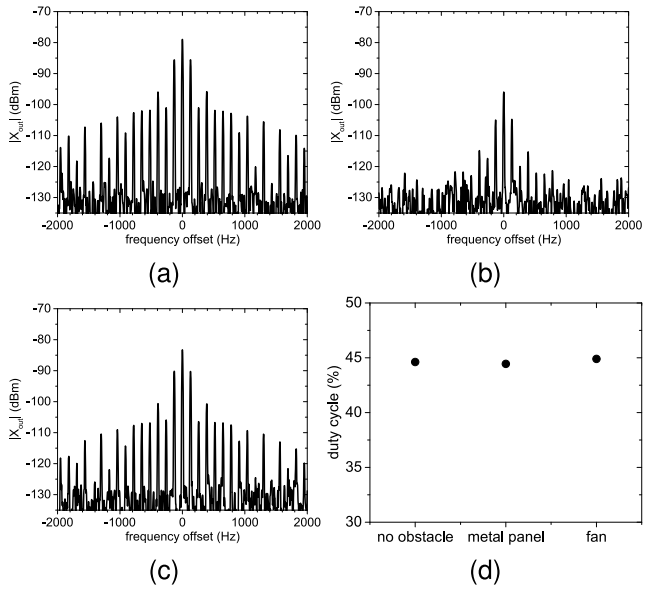

Fig. 17. Experimental results of the wireless vibration sensing system in the presence of obstacles. (a) Acquired spectrum without any obstacle, (b) acquired spectrum with a metal panel between the tag and the reader, (c) acquired spectrum with a rotating fan between the tag and the reader, and (d) measured duty cycle.

the ratio obtained with the right-hand sidebands with the one obtained with the left-hand sidebands. Concerning dynamic multipath, as long as it is slower than the vibration frequency, it does not significantly affect the communication. Fig. 16 shows the experimental setups. First, we put a metal panel (30×50 cm^2) between the reader antennas and the tag (absence of line of sight and strong f_0 reflections), and then we replace the metal panel with a rotating fan. The tag-to-reader distance is 100 cm. The acquired spectrum and measured duty cycle are shown in Fig. 17(a) and (b), respectively. Vibration frequency and acceleration are kept constant in all the experiments. Although attenuated, the acquired spectrum preserves its shape in presence of both types of obstacles, thus confirming the capability of the sensor to operate in harsh environments.

In the present work, we tested the capability of the system to recover the vibration information from a single wireless passive tag. In case multiple transponders are used, they can be separated in the frequency domain, by designing each tag for different RF frequencies and by making the transmitter sweep over frequency.

The presented wireless passive vibration sensor is then compared with other state-of-the-art wireless vibration sensors based on backscatter radios in Table I. The proposed solution features an excellent compromise among low-cost, sensitivity, and versatility, while representing a fully passive wireless solution, and the obtained results open the door to a novel acquisition method for vibration sensing in industrial environments.

IV. CONCLUSION

A novel vibration sensing approach has been presented, based on a passive harmonic transponder and a piezoelectric cantilever. It has been shown that the piezoelectric transducer is able to modulate the amplitude of the harmonic backscattered signal by controlling the gate of an NMOS switch. The vibration frequency is encoded in the frequency difference between the spectral lines of the received signal, while the acceleration is encoded in the duty cycle of the amplitude modulation of the backscattered signal. A method to derive the

sensor information using only the spectrum of the harmonic backscattered signal (scalar noncoherent measurement) has been described in an implementation that does not depend on the tag-to-reader distance. A prototype has been manufactured and tested, and the concept has been proven successfully. This work opens the door to a new class of harmonic wireless passive sensors suitable for industrial applications.

REFERENCES

[1] H. El Matbouly, K. Zannas, Y. Duroc, and S. Tedjini, "Analysis and assessments of time delay constrains for passive RFID tag-sensor communication link: Application for rotation speed sensing," *IEEE Sensors J.*, vol. 17, no. 7, pp. 2174–2181, Apr. 2017.

[2] J. M. Williams et al., "Weaving the wireless web: Toward a low-power, dense wireless sensor network for the industrial IoT," *IEEE Microw. Mag.*, vol. 18, no. 7, pp. 40–63, Nov. 2017.

[3] P. Jayalaxmi, R. Saha, G. Kumar, N. Kumar, and T.-H. Kim, "A taxonomy of security issues in Industrial Internet-of-Things: Scoping review for existing solutions, future implications, and research challenges," *IEEE Access*, vol. 9, pp. 25344–25359, 2021.

[4] I. Koene, R. Viitala, and P. Kuosmanen, "Internet of Things based monitoring of large rotor vibration with a microelectromechanical systems accelerometer," *IEEE Access*, vol. 7, pp. 92210–92219, 2019.

[5] B. Yaghootkar, S. Azimi, and B. Bahreyni, "A high-performance piezoelectric vibration sensor," *IEEE Sensors J.*, vol. 17, no. 13, pp. 4005–4012, Jul. 2017.

[6] R. De Fazio, M. Stabile, M. De Vittorio, R. Velázquez, and P. Visconti, "An overview of wearable piezoresistive and inertial sensors for respiration rate monitoring," *Electronics*, vol. 10, no. 17, p. 2178, Sep. 2021.

[7] A. Sabato, C. Niezrecki, and G. Fortino, "Wireless MEMS-based accelerometer sensor boards for structural vibration monitoring: A review," *IEEE Sensors J.*, vol. 17, no. 2, pp. 226–235, Jan. 2017.

[8] J. Qian et al., "A MEMS fiber-optic Fabry–Perot vibration sensor for high-temperature applications," *IEEE Access*, vol. 10, pp. 42908–42915, 2022.

[9] A. Bighashdel, H. Zare, S. H. Pourtakdoust, and A. A. Sheikhy, "An analytical approach in dynamic calibration of strain gauge balances for aerodynamic measurements," *IEEE Sensors J.*, vol. 18, no. 9, pp. 3572–3579, May 2018.

[10] Z. T. Nishino, K. Chen, and N. Gupta, "Power modulation-based optical sensor for high-sensitivity vibration measurements," *IEEE Sensors J.*, vol. 14, no. 7, pp. 2153–2158, Jul. 2014.

[11] I. Zaitsev et al., "Calculation of capacitive-based sensors of rotating shaft vibration for fault diagnostic systems of powerful generators," *Sensors*, vol. 22, no. 4, p. 1634, Feb. 2022.

[12] S. Roundy, P. K. Wright, and J. Rabaey, "A study of low level vibrations as a power source for wireless sensor nodes," *Comput. Commun.*, vol. 26, no. 11, pp. 1131–1144, Jul. 2003.

[13] A. P. Sample, D. J. Yeager, P. S. Powledge, A. V. Mamishev, and J. R. Smith, "Design of an RFID-based battery-free programmable sensing platform," *IEEE Trans. Instrum. Meas.*, vol. 57, no. 11, pp. 2608–2615, Nov. 2008.

[14] A. Costanzo, F. Benassi, and G. Monti, "Wearable, energy-autonomous RF microwave systems: Chipless and energy-harvesting-based wireless systems for low-power, low-cost localization and sensing," *IEEE Microw. Mag.*, vol. 23, no. 3, pp. 24–38, Mar. 2022.

[15] R. Torres et al., "Backscatter communications," *IEEE J. Microw.*, vol. 1, no. 4, pp. 864–878, Oct. 2021.

[16] P. Mezzanotte, V. Palazzi, F. Alimenti, and L. Roselli, "Innovative RFID sensors for Internet of Things applications," *IEEE J. Microw.*, vol. 1, no. 1, pp. 55–65, Jan. 2021.

[17] J. Kimionis, A. Bletsas, and J. N. Sahalos, "Increased range bistatic scatter radio," *IEEE Trans. Commun.*, vol. 62, no. 3, pp. 1091–1104, Mar. 2014.

[18] N. Fasarakis-Hilliard, P. N. Alevizos, and A. Bletsas, "Coherent detection and channel coding for bistatic scatter radio sensor networking," *IEEE Trans. Commun.*, vol. 63, no. 5, pp. 1798–1810, May 2015.

[19] E. Kampianakis, J. Kimionis, K. Tountas, C. Konstantopoulos, E. Koutroulis, and A. Bletsas, "Wireless environmental sensor networking with analog scatter radio and timer principles," *IEEE Sensors J.*, vol. 14, no. 10, pp. 3365–3376, Oct. 2014.

[20] A. Boaventura, J. Santos, A. Oliveira, and N. B. Carvalho, "Perfect isolation: Dealing with self-jamming in passive RFID systems," *IEEE Microw. Mag.*, vol. 17, no. 11, pp. 20–39, Nov. 2016.

[21] C. Konstantopoulos, E. Koutroulis, N. Mitianoudis, and A. Bletsas, "Converting a plant to a battery and wireless sensor with scatter radio and ultra-low cost," *IEEE Trans. Instrum. Meas.*, vol. 65, no. 2, pp. 388–398, Feb. 2016.

[22] S.-N. Daskalakis, S. D. Assimonis, E. Kampianakis, and A. Bletsas, "Soil moisture scatter radio networking with low power," *IEEE Trans. Microw. Theory Techn.*, vol. 64, no. 7, pp. 2338–2346, Jul. 2016.

[23] G. Vannucci, A. Bletsas, and D. Leigh, "A software-defined radio system for backscatter sensor networks," *IEEE Trans. Wireless Commun.*, vol. 7, no. 6, pp. 2170–2179, Jun. 2008.

[24] V. Viikari, H. Seppa, and D.-W. Kim, "Intermodulation read-out principle for passive wireless sensors," *IEEE Trans. Microw. Theory Techn.*, vol. 59, no. 4, pp. 1025–1031, Apr. 2011.

[25] J. Yao, Y. M. Hew, A. Mears, and H. Huang, "Strain gauge-enable wireless vibration sensor remotely powered by light," *IEEE Sensors J.*, vol. 15, no. 9, pp. 5185–5192, Sep. 2015.

[26] J. Yao, S. Tjuatja, and H. Huang, "Real-time vibratory strain sensing using passive wireless antenna sensor," *IEEE Sensors J.*, vol. 15, no. 8, pp. 4338–4345, Aug. 2015.

[27] W. Wang, X. Xue, Y. Huang, and X. Liu, "A novel wireless and temperature-compensated SAW vibration sensor," *Sensors*, vol. 14, no. 11, pp. 20702–20712, Nov. 2014.

[28] C. Li, Y. Xue, P. Jia, M. Jia, B. Sun, and J. Xiong, "A wireless passive vibration sensor based on high-temperature ceramic for harsh environment," *J. Sensors*, vol. 2021, Jan. 2021, Art. no. 8875907.

[29] I. T. Nassar, J. Wang, J. L. Frolik, and T. M. Weller, "A high-efficiency, miniaturized sensor node with 3-D machined-substrate antennas for embedded wireless monitoring," *IEEE Sensors J.*, vol. 15, no. 9, pp. 5036–5044, Sep. 2015.

[30] B. Yan et al., "Indoor photovoltaics awaken the world's first solar cells," *Sci. Adv.*, vol. 8, no. 49, Dec. 2022, Art. no. eadc9923.

[31] D. Mandal and S. Banerjee, "Surface acoustic wave (SAW) sensors: Physics, materials, and applications," *Sensors*, vol. 22, no. 3, p. 820, Jan. 2022.

[32] J. R. Riley et al., "Tracking bees with harmonic radar," *Nature*, vol. 379, no. 6560, pp. 29–30, Jan. 1996.

[33] X. Gu, N. N. Srinaga, L. Guo, S. Hemour, and K. Wu, "Diplexer-based fully passive harmonic transponder for sub-6-GHz 5G-compatible IoT applications," *IEEE Trans. Microw. Theory Techn.*, vol. 67, no. 5, pp. 1675–1687, May 2019.

[34] V. Palazzi, L. Roselli, M. M. Tentzeris, P. Mezzanotte, and F. Alimenti, "Energy-efficient harmonic transponder based on on-off keying modulation for both identification and sensing," *Sensors*, vol. 22, no. 2, p. 620, Jan. 2022.

[35] V. Palazzi, F. Alimenti, P. Mezzanotte, G. Orecchini, and L. Roselli, "Zero-power, long-range, ultra low-cost harmonic wireless sensors for massively distributed monitoring of cracked walls," in *IEEE MTT-S Int. Microw. Symp. Dig.*, Jun. 2017, pp. 1335–1338.

[36] S. Mondal, D. Kumar, and P. Chahal, "A wireless passive pH sensor with clutter rejection scheme," *IEEE Sensors J.*, vol. 19, no. 9, pp. 3399–3407, May 2019.

[37] X. Hui, T. B. Conroy, and E. C. Kan, "Near-field coherent sensing of vibration with harmonic analysis and balance signal injection," *IEEE Trans. Microw. Theory Techn.*, vol. 69, no. 3, pp. 1906–1916, Mar. 2021.

[38] T. M. Silveira, P. Pinho, and N. B. Carvalho, "Harmonic RFID temperature sensor design for harsh environments," *IEEE Microw. Wireless Compon. Lett.*, vol. 32, no. 10, pp. 1239–1242, Oct. 2022.

[39] R. Raju and G. E. Bridges, "A compact wireless passive harmonic sensor for packaged food quality monitoring," *IEEE Trans. Microw. Theory Techn.*, vol. 70, no. 4, pp. 2389–2397, Apr. 2022.

[40] A. Abdelnour, A. Lazaro, R. Villarino, D. Kaddour, S. Tedjini, and D. Girbau, "Passive harmonic RFID system for buried assets localization," *Sensors*, vol. 18, no. 11, p. 3635, Oct. 2018.

[41] V. Palazzi et al., "Low-power frequency doubler in cellulose-based materials for harmonic RFID applications," *IEEE Microw. Wireless Compon. Lett.*, vol. 24, no. 12, pp. 896–898, Dec. 2014.

[42] C. Covaci and A. Gontean, "Piezoelectric energy harvesting solutions: A review," *Sensors*, vol. 20, no. 12, p. 3512, Jun. 2020.

[43] H. Li, C. Tian, and Z. D. Deng, "Energy harvesting from low frequency applications using piezoelectric materials," *Appl. Phys. Rev.*, vol. 1, no. 4, Dec. 2014, Art. no. 041301.
[44] W. Wang, T. Yang, X. Chen, and X. Yao, "Vibration energy harvesting using a piezoelectric circular diaphragm array," *IEEE Trans. Ultrason., Ferroelectr., Freq. Control*, vol. 59, no. 9, pp. 2022–2026, Sep. 2012.

Valentina Palazzi (Senior Member, IEEE) received the M.S. degree in electrical engineering and the Ph.D. degree in industrial and information engineering from the University of Perugia, Perugia, Italy, in 2014 and 2018, respectively.

In 2015, she was a Visiting Ph.D. Student with the Tyndall National Institute, Cork, Ireland; in 2016, she did a short-term scientific mission with the Centre Tecnològic de Telecomunicacions de Catalunya, Barcelona, Spain, sponsored by the cost action IC1301 "WiPE"; from December 2016 to April 2017, she was a Student Intern with the Agile Technologies for High-Performance Electromagnetic Novel Applications Research Group, School of Electrical and Computer Engineering, Georgia Institute of Technology, Atlanta, GA, USA. Since 2019, she has been a Researcher with the High Frequency Electronics Laboratory, Department of Engineering, University of Perugia. She has coauthored more than 60 articles and holds three patents. Her current research interests include RF components, wireless sensors, radar front-ends, wireless power transfer technologies, additive manufacturing processes, and conformal electronics.

Dr. Palazzi was a recipient of the First Place Award of the Student Design Competition on Wireless Energy Harvesting held at the 2016 IEEE MTT-S "International Microwave Symposium" (IMS), the IEEE MTT-S Graduate Fellowship in 2017, the 2017 MTT-S Prize—Italy Chapter Central and Southern Italy, the URSI Young Scientist Best Paper Award conferred at the 2019 URSI Italian National Meeting, the Second Place at the 3 Minute Thesis Competition held at IMS 2021, and the GAAS Young Scientist Recognition (URSI Commission D) conferred at GASS 2021. She is the Chair of the IEEE MTT-S Technical Committee–26 "RFID, Wireless Sensor and IoT" from 2022 to 2023, and the Early Career Representative of the Commission D "Electronics and Photonics" of the International Union of Radio Science (URSI) from 2021 to 2026. She is the Secretary of 2023 IEEE Microwave Theory and Technology Society (MTT-S).

Federico Alimenti (Senior Member, IEEE) received the Laurea degree (magna cum laude) and Ph.D. degree in electronic engineering from the University of Perugia, Perugia, Italy, in 1993 and 1997, respectively.

In 1996, he was a Visiting Scientist at the Technical University of Munich, Munich, Germany. Since 2001, he has been with the Department of Engineering, University of Perugia, teaching the class of RFIC Design. From 2011 to 2014, he was the Scientific Coordinator of the ENIAC ARTEMOS Project. In the summer 2014, he was a Visiting Professor at EPFL, Lausanne, Switzerland. He has participated at the Summer School 2017, held at Infineon Austria AG, Villach, Austria, as a Keynote Lecturer. He has authored a European Patent (EP2660755) and more than 200 papers in journals conferences and books. The H-index of Federico Alimenti is 26 with more than 2400 citations (source Scopus). His research interests include microwave and RFIC design.

Dr. Alimenti was a recipient of the URSI Young Scientist Award, the IET Premium (Best Paper) Award in 2013, and he got the qualification as "Full Professor" and won the "Mario Sannino" Award for the best research in the field of microwave electronics, in 2018. He was the TPC Chair of the IEEE Wireless Power Transfer Conference.

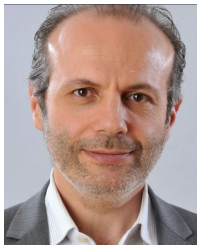

Paolo Mezzanotte (Member, IEEE) was born in Perugia, Italy, in 1965. He received the Ph.D. degree from the University of Perugia, Perugia, in 1997.

Since 2007, he has been an Associate Professor with the University of Perugia, where he has been involved in teaching the classes "Radio-Frequencies Engineering" and "Systems and Circuits for IoT." His present H-index is 26 (source Scopus). His current research interests include the development of microwave circuits on biocompatible substrates and the enabling technologies for IoT. These research activities are testified by more than 170 publications in the most reputed specialized journals and at the main conferences of the microwave scientific community.

Dr. Mezzanotte served as the Chair for the IEEE Technical Committee MTT-24-RFID Technologies for the biennium from 2018 to 2019. He is the Chair of the IEEE Topical Conference on Wireless Sensors and Sensor Networks (WiSNet). He was the Vice Head of the Department of Engineering, University of Perugia, from 2014 to 2019. He is an Associate Editor of *ACES journal* and IEEE JOURNAL OF MICROWAVES.

Manos M. Tentzeris (Fellow, IEEE) received the Diploma degree (magna cum laude) in electrical and computer engineering from the National Technical University of Athens, Athens, Greece, in 1992, and the M.S. and Ph.D. degrees in electrical engineering and computer science from the University of Michigan, Ann Arbor, MI, USA, in 1993 and 1998, respectively.

He was a Visiting Professor with the Technical University of Munich, Munich, Germany, in 2002; the GTRI-Ireland, Athlone, Ireland, in 2009; and the LAAS-CNRS, Toulouse, France, in 2010. He has served as the Head of the GTECE Electromagnetics Technical Interest Group, the Georgia Electronic Design Center Associate Director of RFID/Sensors Research, the Georgia Institute of Technology NSF-Packaging Research Center Associate Director of RF Research, and the RF Alliance Leader. He is currently a Ken Byers Professor of flexible electronics with the School of Electrical and Computer Engineering, Georgia Institute of Technology, Atlanta, GA, USA, where he heads the ATHENA Research Group (20 researchers). He has helped develop academic programs in 3-D/inkjet-printed RF electronics and modules, flexible electronics, origami and morphing electromagnetics, highly integrated/multilayer packaging for RF, millimeter-wave, sub-THz and wireless applications using ceramic and organic flexible materials, paper-based RFID's and sensors, wireless sensors and biosensors, wearable electronics, "Green" electronics, energy harvesting and wireless power transfer, nanotechnology applications in RF, microwave MEMs, and SOP-integrated (UWB, multiband, mmW, and conformal) antennas. He has authored more than 850 articles in refereed journals and conference proceedings, seven books, and 26 book chapters. He has given more than 100 invited talks to various universities and companies all over the world.

Dr. Tentzeris is a member of the URSI-Commission D and the MTT-15 Committee, an Associate Member of EuMA, a Fellow of the Electromagnetic Academy, and a member of the Technical Chamber of Greece. He was a recipient/co-recipient of the 2022 Georgia Tech Outstanding Doctoral Thesis Advisor Award, the 2019 Humboldt Research Prize, the 2017 Georgia Institute of Technology Outstanding Achievement in Research Program Development Award, the 2016 Bell Labs Award Competition 3rd Prize, the 2015 IET Microwaves, Antennas, and Propagation Premium Award, the 2014 Georgia Institute of Technology ECE Distinguished Faculty Achievement Award, the 2014 IEEE RFID-TA Best Student Paper Award, the 2013 IET Microwaves, Antennas and Propagation Premium Award, the 2012 FiDiPro Award in Finland, the iCMG Architecture Award of Excellence, the 2010 IEEE Antennas and Propagation Society Piergiorgio L.E. Uslenghi Letters Prize Paper Award, the 2011 International Workshop

on Structural Health Monitoring Best Student Paper Award, the 2010 Georgia Institute of Technology Senior Faculty Outstanding Undergraduate Research Mentor Award, the 2009 IEEE TRANSACTIONS ON COMPONENTS AND PACKAGING TECHNOLOGIES Best Paper Award, the 2009 E. T. S. Walton Award from the Irish Science Foundation, the 2007 IEEE AP-S Symposium Best Student Paper Award, the 2007 IEEE MTT-S IMS Third Best Student Paper Award, the 2007 ISAP 2007 Poster Presentation Award, the 2006 IEEE MTT-S Outstanding Young Engineer Award, the 2006 Asia–Pacific Microwave Conference Award, the 2004 IEEE TRANSACTIONS ON ADVANCED PACKAGING Commendable Paper Award, the 2003 NASA Godfrey "Art" Anzic Collaborative Distinguished Publication Award, the 2003 IBC International Educator of the Year Award, the 2003 IEEE CPMT Outstanding Young Engineer Award, the 2002 International Conference on Microwave and Millimeter-Wave Technology Best Paper Award (Beijing, China), the 2002 Georgia Institute of Technology–ECE Outstanding Junior Faculty Award, the 2001 ACES Conference Best Paper Award, the 2000 NSF CAREER Award, and the 1997 Best Paper Award of the International Hybrid Microelectronics and Packaging Society. He was the TPC Chair of the IEEE MTT-S IMS 2008 Symposium and the Chair of the 2005 IEEE CEM-TD Workshop. He is the Vice-Chair of the RF Technical Committee (TC16) of the IEEE CPMT Society. He is the Founder and the Chair of the RFID Technical Committee (TC24) of the IEEE MTT-S and the Secretary/Treasurer of the IEEE C-RFID. He served as one of the IEEE MTT-S Distinguished Microwave Lecturers from 2010 to 2012 and the IEEE CRFID Distinguished Lectures. He is an Associate Editor of IEEE TRANSACTIONS ON MICROWAVE THEORY AND TECHNIQUES, the IEEE TRANSACTIONS ON ADVANCED PACKAGING, and the *International Journal on Antennas and Propagation*.

Luca Roselli (Fellow, IEEE) joined the University of Perugia, Perugia, Italy, in 1991. In 2000, he founded the spin-off WiS Srl, Foligno, PG, Italy. He was involved in electronic technologies for Internet of Things for more than six years. He is currently a Full Professor with the University of Perugia, where he teaches applied electronics and coordinates the High Frequency Electronics Laboratory. He has authored more than 280 articles (H-i 37, i10 117, more than 4800 citations-Scholar) and *Green RFID System* (Cambridge University Press, 2014). His current research interests include HF electronic systems with a special attention to RFID, new materials, and wireless power transfer.

Dr. Roselli was a member of the Board of Directors of ART Srl, Urbino, Italy, from 2008 to 2012. He is a member of the list of experts of the Italian Ministry of Research, the past Chair of the IEEE Technical Committees MTT-24-RFID, the past Chair of 25-RF Nanotechnologies, the Chair of 25-Wireless Power Transfer, the ERC Panel PE7, the Advisory Committee of the IEEE-WPTC, and the Chair of the SC-32 of IMS. He is the past Co-Chair of the IEEE Wireless Sensor Network Conference. He organized the VII Computational Electromagnetic Time Domain in 2007 and the first IEEE Wireless Power Transfer Conference in 2013. He is an Associate Editor of *IEEE Microwave Magazine*. He is involved on the boards of several international conferences. He is a reviewer for many international reviews, including the PROCEEDINGS OF THE IEEE, IEEE TRANSACTIONS ON MICROWAVE THEORY AND TECHNIQUES, and IEEE MICROWAVE AND WIRELESS COMPONENTS LETTERS.